



Supplement of

Ocean acidification trends and carbonate system dynamics across the North Atlantic subpolar gyre water masses during 2009–2019

David Curbelo-Hernández et al.

Correspondence to: Melchor González-Dávila (melchor.gonzalez@ulpgc.es)

The copyright of individual parts of the supplement might differ from the article licence.

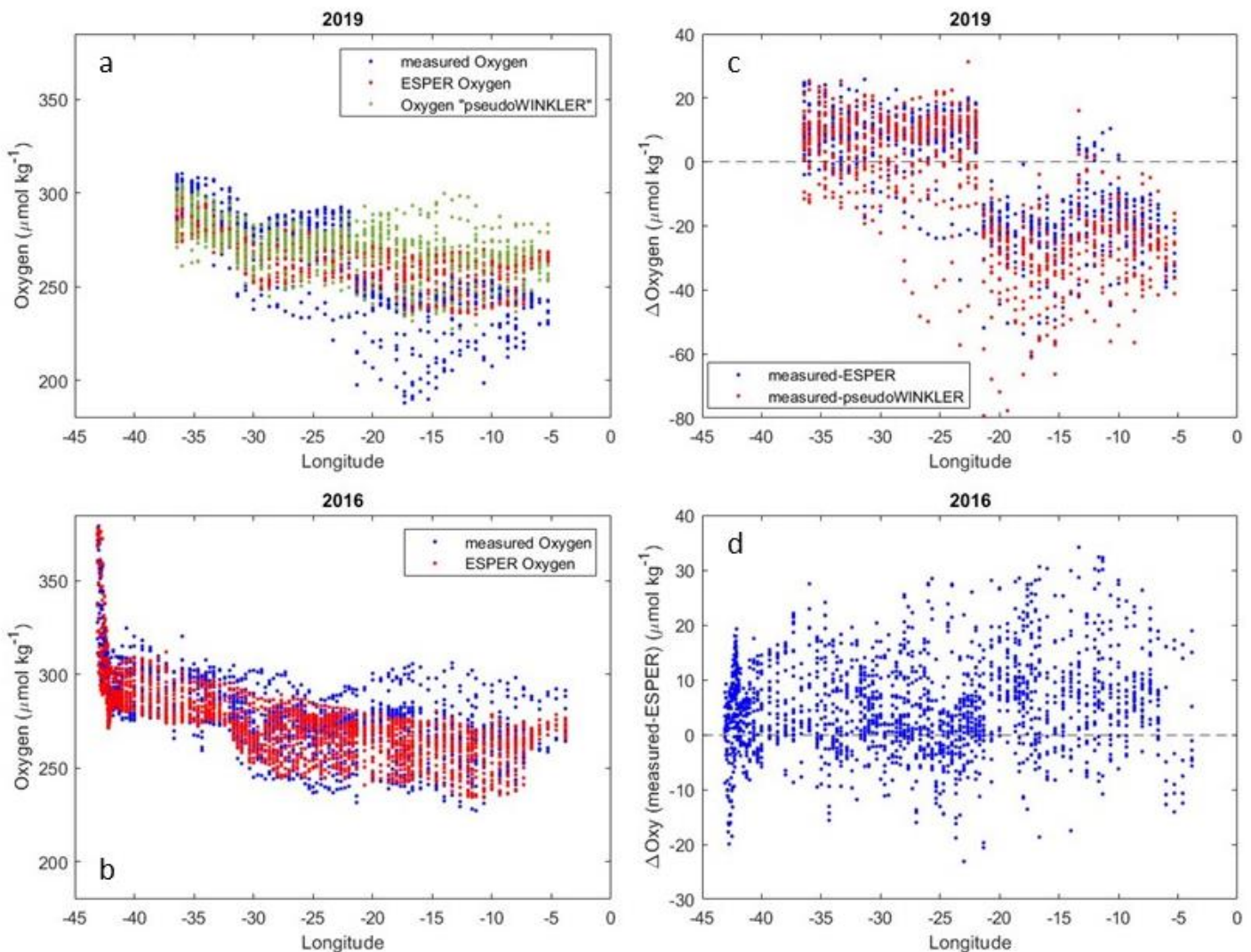


Figure S1. Longitudinal distribution of (a) sensor-measured, ESPER-estimated and pseudo-WINKLER oxygen data for 2019, (b) WINKLER-measured and ESPER-estimated data for 2016, (c) $\Delta\text{DO}_{\text{meas-ESP}}$ and $\Delta\text{DO}_{\text{meas-pseudoWINLKER}}$ for the cruise of 2019 and (d) $\Delta\text{DO}_{\text{meas-ESP}}$ for the cruise of 2016.

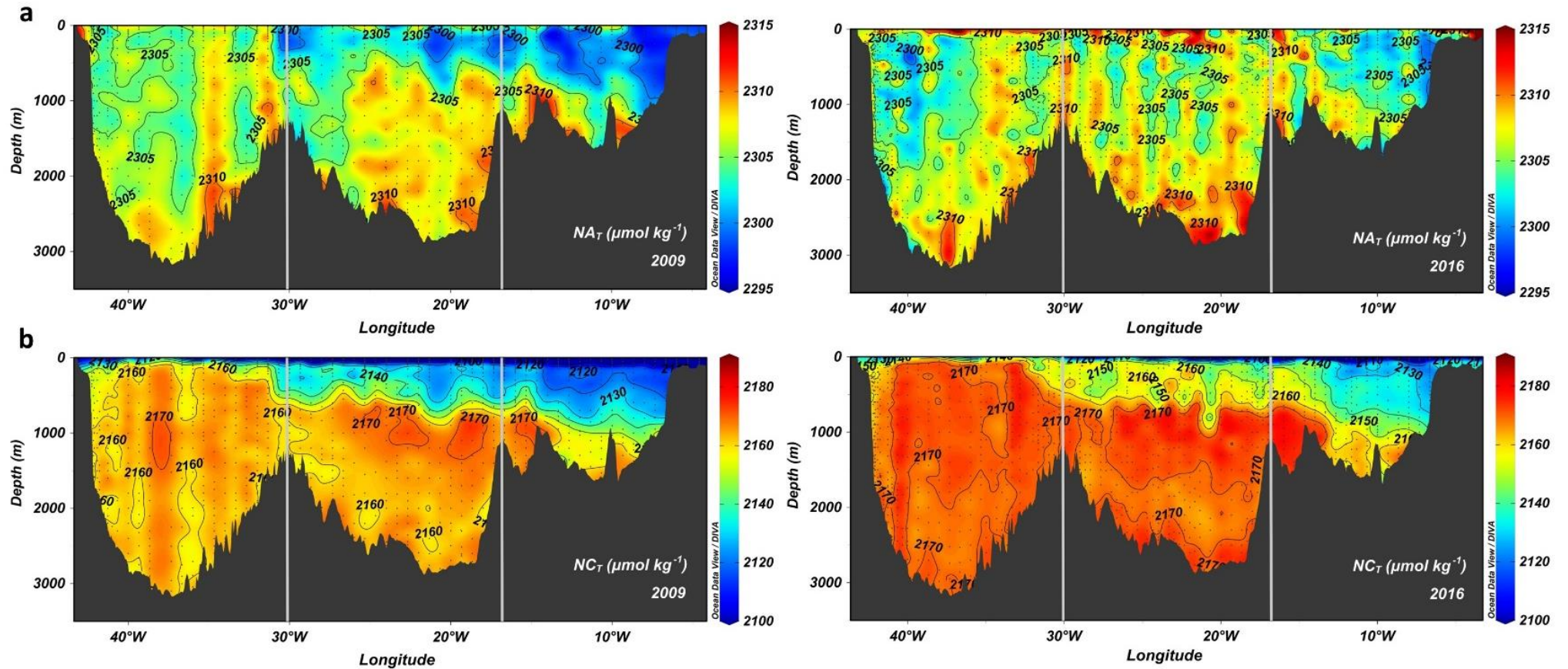


Figure S2. Water-column distribution along the longitudinal transect of (a) NA_T and (b) NC_T for the cruises of 2009 (left plots) and 2016 (right plots). The vertical white lines show the limits between basins. Figure produced with Ocean Data View (Schlitzer, Reiner, Ocean Data View, <https://odv.awi.de>, 2021).

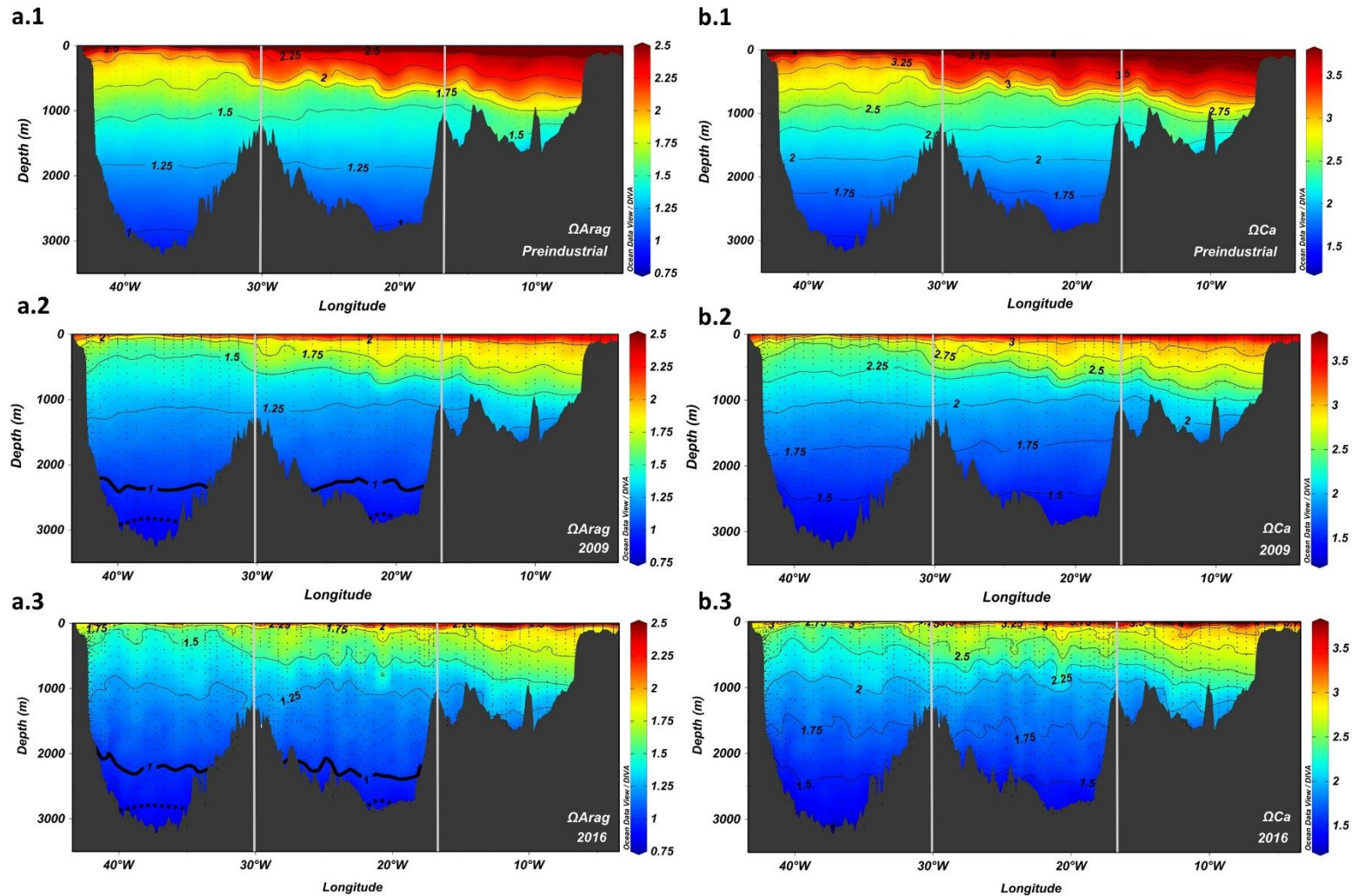


Figure S3. Water-column distribution along the longitudinal transect of (a) Ω_{Arag} and (b) Ω_{Ca} for preindustrial times and for the cruises of 2009 and 2016. The preindustrial Ω_{Arag} and Ω_{Ca} values were computed with the CO₂sys programme (Lewis and Wallace, 1998) run with the MATLAB software (van Heuven et al., 2011; Orr et al., 2018; Sharp et al., 2023) using as input CO₂ system variables the A_T and the C_{nat}. In panels a.2 and a.3, the highlighted continuous black isolines represent the aragonite saturation state horizon during the cruises of 2009 and 2016, respectively, while dash isolines show the aragonite saturation state horizon in preindustrial times. The vertical white lines show the limits between basins. Figure produced with Ocean Data View (Schlitzer, Reiner, Ocean Data View, <https://odv.awi.de>, 2021).

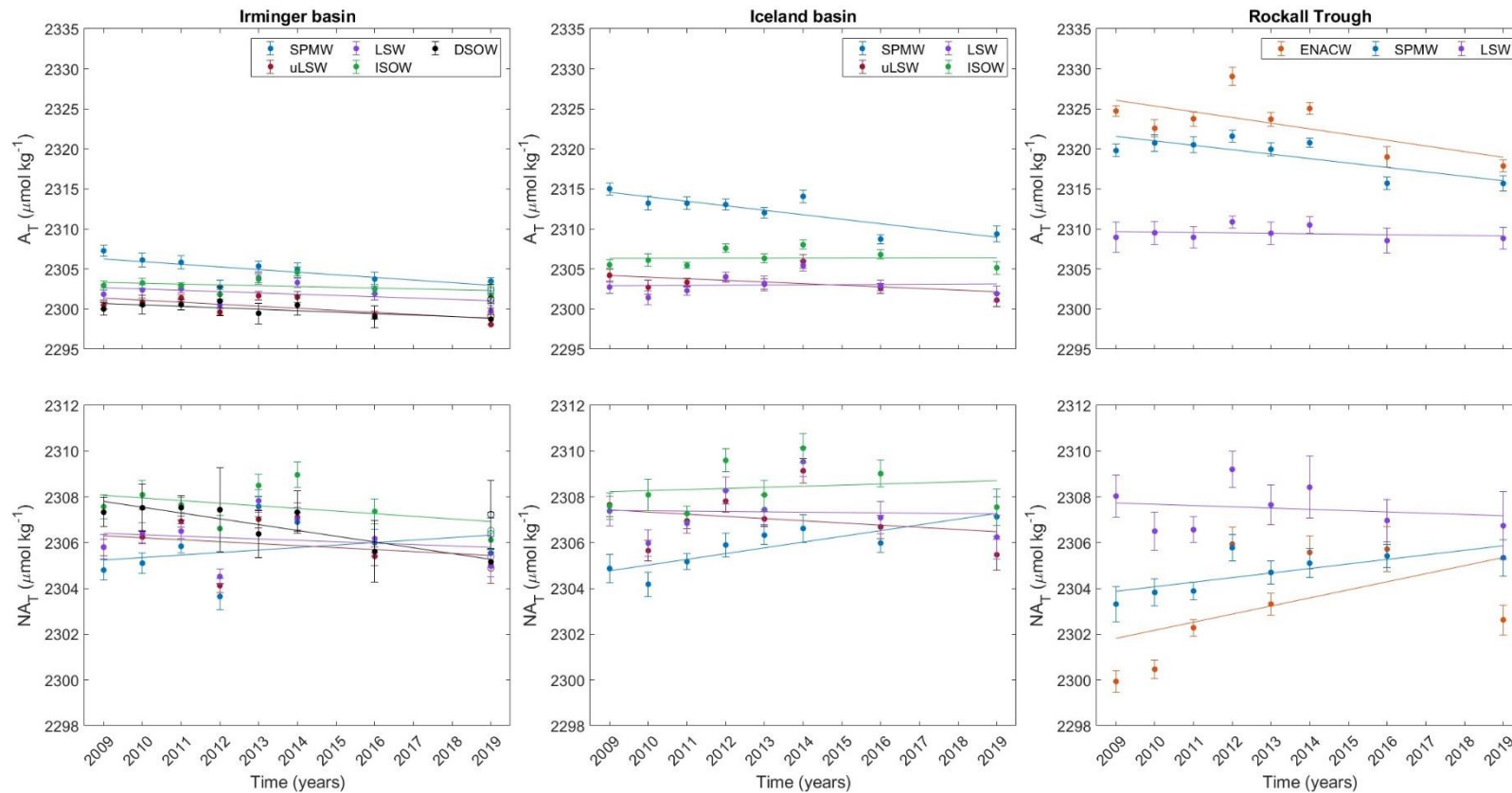


Figure S4. Temporal distribution (2009-2019) of the average A_T and NAt in each of the layers considered for the Irminger (left plot column), Iceland (central plot column) and Rockall basins (right plot column). The average values were calculated for each cruise and layer and represented with coloured points together with their respective error bars at the time of each cruise (the method used for calculations was described in section 3.2). In the Irminger plots, the empty points represent the average values for 2019 calculated with the measured data available in the easternmost part of the basin (sampled part during this cruise), while the coloured points for 2019 represent the average values corrected with A25-OVIDE-2018 data. The interannual trend were given by linear regression of the average values, with the values of the slope, the standard error of estimate and the r^2 presented in Table S4.

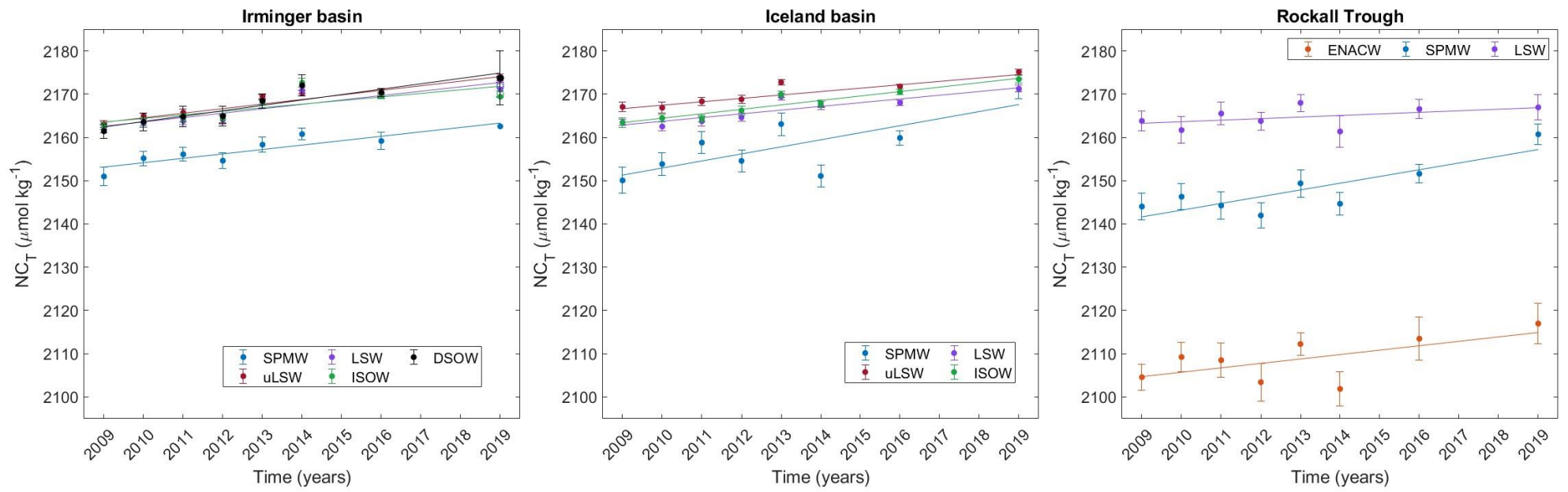


Figure S5. Same as Figure S4 but for NC_T .

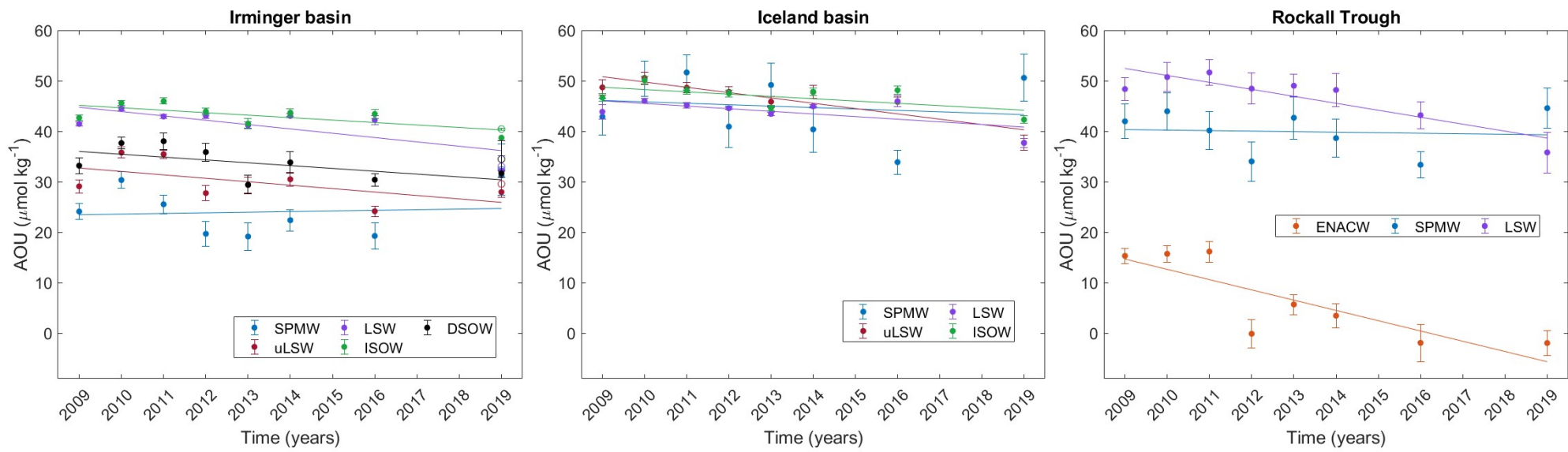


Figure S6. Same as Figure S4 but for AOU.

Table S1. Amount of data (n), mean values and standard deviation (std) per cruise for the measured temperature, salinity, A_T, C_T, pH_T, DO, PO₄ and Si(OH)₄.

Cruise	Temperature (°C)			Salinity			A _T ($\mu\text{mol kg}^{-1}$)			C _T ($\mu\text{mol kg}^{-1}$)			pH _T			DO ($\mu\text{mol kg}^{-1}$)			PO ₄ ($\mu\text{mol kg}^{-1}$)			Si(OH) ₄ ($\mu\text{mol kg}^{-1}$)		
	n	mean	std	n	mean	std	n	mean	std	n	mean	std	n	mean	std	n	mean	std	n	mean	std	n	mean	std
2009	1307	6.509	2.966	1307	35.094	0.177	1087	2308.5	12.8	559	2149.3	20.2	975	8.0066	0.0387	1297	266.8	16.7	1319	0.96	0.22	1326	8.83	3.44
2010	1192	6.711	3.233	1192	35.089	0.173	870	2309.7	9.0	763	2151.8	23.5	1071	7.9978	0.0365	1178	261.3	15.7	1220	0.88	0.27	1228	8.42	3.96
2011	1279	5.979	2.770	1279	35.055	0.156	1080	2308.4	9.5	851	2154.1	21.1	1035	7.9994	0.0350	1167	266.2	15.4	1284	0.92	0.23	1284	8.67	3.72
2012	1205	5.867	2.541	1205	35.056	0.159	1189	2308.3	12.5	900	2152.9	20.8	1126	8.0105	0.0438	1136	272.9	17.6	1163	0.91	0.21	1158	8.22	3.49
2013	1235	6.354	2.592	1235	35.057	0.158	1324	2306.8	15.3	1206	2154.4	19.4	1199	8.0077	0.0394	1223	272.3	19.0	1248	0.90	0.21	1279	7.56	3.73
2014	1226	6.476	2.889	1226	35.068	0.157	1059	2307.7	16.1	983	2151.0	25.5	1196	8.0089	0.0454	1211	271.3	16.5	1272	0.90	0.27	1275	6.82	3.67
2016	1849	5.514	2.253	1849	35.001	0.114	1557	2305.6	8.2	1465	2157.9	19.0	1349	7.9959	0.0415	1676	276.1	16.5	1608	0.96	0.23	1642	7.49	2.97
2019	768	6.721	3.146	768	35.042	0.126	808	2307.3	8.6	768	2155.3	28.6	755	7.9796	0.0480	768	271.4	16.2	-	-	-	-	-	-

Table S2. Comparison of measured variables with canyon-estimated and CO₂sys-computed variables for each cruise. The table shows the number of measured data points (n), the mean differences between measurements and calculations, and the standard deviation (std). An internal consistency test, comparing measured and computed variables, was conducted for cruises between 2009 and 2016, where three MCS variables were measured. For the computations, pH_T and C_T were used as input variables for A_T, A_T and C_T for pH_T, and A_T and pH_T for C_T.

Table S3. Amount (n) and percentage of measured and computed C_T data per cruise used to compile the C_T "new". No computed C_T data were used for the 2019 cruise due to lack of measured pH needed for computation.

Cruise	C_T "new"					
	n total	C_T measured		C_T computed		
		n	percentage	n	percentage	
2009	1088	501	46.05%	587	53.95%	
2010	1202	709	58.98%	493	41.02%	
2011	1029	645	62.68%	384	37.32%	
2012	1161	735	63.31%	426	36.69%	
2013	1307	1095	83.78%	212	16.22%	
2014	1285	713	55.49%	572	44.51%	
2016	1421	1223	86.07%	198	13.93%	
2019	754	754	100%	0	0%	

Table S4. Interannual trends of A_T , NA_T , NC_T and AOU in each of the layers and basins. The ratios of change were based on linear regressions applied to the average values (as represented in Supplementary Figures 2-4) and presented together with its Standard error of estimate. The correlation coefficients r^2 and p-values were also provided. Values in bold denotes that trends are statistically significant at the 95% level of confidence.

Basin	Layer	A_T			NA_T			NC_T			AOU		
		ratio ($\mu\text{mol kg}^{-1} \text{yr}^{-1}$)	r^2	p-value	ratio ($\mu\text{mol kg}^{-1} \text{yr}^{-1}$)	r^2	p-value	ratio ($\mu\text{mol kg}^{-1} \text{yr}^{-1}$)	r^2	p-value	ratio ($\mu\text{mol kg}^{-1} \text{yr}^{-1}$)	r^2	p-value
Irminger	SPMW	-0.33 \pm 0.17	0.50	0.05	0.13 \pm 0.18	0.12	0.41	1.05 \pm 0.25	0.82	<0.01	-0.79 \pm 0.47	0.43	0.08
	uLSW	-0.16 \pm 0.13	0.27	0.19	-0.04 \pm 0.16	0.02	0.76	1.14 \pm 0.20	0.89	<0.01	-0.80 \pm 0.48	0.42	0.08
	LSW	-0.11 \pm 0.18	0.09	0.47	-0.02 \pm 0.15	0.00	0.90	1.08 \pm 0.24	0.85	<0.01	-0.89 \pm 0.41	0.55	0.04
	ISOW	-0.05 \pm 0.13	0.04	0.64	-0.05 \pm 0.12	0.05	0.61	0.90 \pm 0.33	0.66	<0.01	-0.49 \pm 0.26	0.48	0.05
	DSOW	-0.18 \pm 0.09	0.53	0.04	-0.24 \pm 0.07	0.75	<0.01	1.28 \pm 0.23	0.89	<0.01	-0.62 \pm 0.40	0.38	0.10
Iceland	SPMW	-0.56 \pm 0.19	0.70	<0.01	0.25 \pm 0.08	0.72	<0.01	1.63 \pm 0.70	0.59	0.03	-0.28 \pm 0.98	0.02	0.73
	uLSW	-0.20 \pm 0.19	0.22	0.24	-0.10 \pm 0.18	0.07	0.53	0.79 \pm 0.25	0.72	<0.01	-1.05 \pm 0.28	0.79	<0.01
	LSW	0.02 \pm 0.20	0.00	0.88	-0.02 \pm 0.18	0.00	0.92	0.86 \pm 0.22	0.80	<0.01	-0.52 \pm 0.32	0.40	0.09
	ISOW	0.01 \pm 0.16	0.00	0.96	0.05 \pm 0.16	0.02	0.72	1.03 \pm 0.16	0.91	<0.01	-0.45 \pm 0.29	0.38	0.10
Rockall	ENACW	-0.71 \pm 0.41	0.44	0.07	0.35 \pm 0.32	0.24	0.21	1.02 \pm 0.63	0.41	0.09	-2.03 \pm 0.69	0.70	<0.01
	SPMW	-0.55 \pm 0.22	0.62	0.02	0.20 \pm 0.09	0.54	0.04	1.56 \pm 0.50	0.72	<0.01	-0.10 \pm 0.66	0.01	0.85
	LSW	-0.05 \pm 0.13	0.05	0.61	-0.06 \pm 0.15	0.03	0.66	0.36 \pm 0.33	0.24	0.22	-1.38 \pm 0.37	0.78	<0.01